Earth and Planetary Science Letters 571 (2021) 117112

Contents lists available at ScienceDirect

Earth and Planetary Science Letters

www.elsevier.com/locate/epsl

Recycling of nitrogen and light noble gases in the Central American subduction zone: Constraints from $^{15}N^{15}N$

J. Labidi [a,*], E.D. Young [b], T.P. Fischer [c], P.H. Barry [d], C.J. Ballentine [e], J.M. de Moor [c,f]

[a] Université de Paris, Institut de physique du globe de Paris, CNRS, Paris, France
[b] Department of Earth, Planetary, and Space Sciences, UCLA, Los Angeles, CA, USA
[c] Department of Earth and Planetary Sciences, University of New Mexico, Albuquerque, NM 87131-1116, USA
[d] Marine Chemistry and Geochemistry Department, Woods Hole Oceanographic Institution, Woods Hole, MA 02543, USA
[e] Department of Earth Sciences, University of Oxford, OX1 3AN, UK
[f] Observatorio Volcanológico y Sismológico de Costa Rica (OVSICORI), Universidad Nacional, Costa Rica

ARTICLE INFO

Article history:
Received 11 February 2021
Received in revised form 5 July 2021
Accepted 9 July 2021
Available online xxxx
Editor: R. Hickey-Vargas

Keywords:
nitrogen isotopologues
subduction of volatiles
Central American arc

ABSTRACT

How much nitrogen and light noble gases are recycled in modern subduction zones is unclear. Fumaroles act as a means for passive degassing in arcs. They receive variable contributions of volatiles from arc magmas, themselves sourced from the mantle wedge. The gas compositions reflect the extent of volatile enrichment in sub-arc mantle sources and constrain slab dehydration. However, contributions from atmospheric components in fumaroles are unavoidable. For N_2, neon and argon, the atmospheric components are challenging to discern from slab-derived components. Here, we report $^{15}N^{15}N$ measurements from eight fumaroles and seven bubbling springs, along the Central American arc. Our new $^{15}N^{15}N$ data are coupled with noble gases measurements and show that air-derived components in volcanic gas discharges can easily be underestimated, in both fumaroles and springs, using conventional stable isotope or noble gases methods. We show that, in the absence of $^{15}N^{15}N$ data, previously used tracers for air (e.g., $\delta^{15}N$, N_2/Ar, N_2/He, among others) may lead to erroneous conclusions regarding the origin of volatiles in mixed gases. In contrast, $^{15}N^{15}N$ data provide quantitative constraints on the nature and contributions of both atmospheric and magmatic components. Most springs are heavily dominated by air-derived N_2, while fumaroles show substantial contributions of volcanic endmembers. Based on the fumarole data, we show that magma sources beneath the central American arc are enriched in all volatiles relative to ^{3}He, by two to three orders of magnitude compared to the MORB source. We use new $^{15}N^{15}N$ data to obtain source $N_2/^3$He, ^{3}He/^{36}Ar and ^{3}He/^{22}Ne ratios which we then use to compute volcanic N_2, Ar and Ne degassing fluxes. Using this approach, we show that outgassing fluxes appear to match subduction fluxes in the Central America subduction zone. We determine an N_2 outgassing flux of between 4.0×10^8 and 1.0×10^9 mol N_2/y, comparable to the subduction flux of 5.7×10^8 mol N_2/yr determined previously. We obtain a similar conclusion for ^{22}Ne and ^{36}Ar. Overall, the volatile fluxes in the central American subduction zone no longer seem to require net transfer of N_2, Ar, and Ne, to the deep mantle.

1. Introduction

The origin of volatiles emitted from convergent margins provides fundamental constraints on how plate tectonics redistributes volatiles between terrestrial reservoirs (Bekaert et al., 2021; Hilton et al., 2002; Plank et al., 2013). The nitrogen cycle is underconstrained, partly because quantifying degassing N_2 fluxes in arcs is challenging. For instance, basalt glasses are virtually absent in subduction zones, impeding quantification of nitrogen elemental abundances in the underlying mantle wedge. The systematic study of metamorphic rocks has suggested nitrogen is quantitatively retained within minerals in downgoing slabs (Bebout et al., 2013; Busigny et al., 2003). The latter is based on the composition of rocks from the European alps, where sediments underwent metamorphism in a cold subduction zone (630 °C at 100 km, Busigny et al., 2003). In those rocks, nitrogen is hosted in the structures of clay minerals including micas and illites, as NH_4^+ substituting for potassium (Bebout and Fogel, 1992; Busigny et al., 2003). Experimental work confirms that the fluid/rock nitrogen partition coefficient in a cold P-T pathway is in favor of N retention in

* Corresponding author.
E-mail address: labidi@ipgp.fr (J. Labidi).

https://doi.org/10.1016/j.epsl.2021.117112
0012-821X/

minerals (Jackson et al., 2021). However, under warmer conditions, fluid/rock partitioning favors N accumulation in fluids, potentially limiting nitrogen subduction to the mantle (Jackson et al., 2021). Subduction temperature gradients were likely steeper in most of the Proterozoic and Archean (Martin and Moyen, 2002). Therefore, it is unclear how modern fluxes determined in cold subduction zones should be extrapolated back into deep time.

The Central American Volcanic Arc (CAVA) is relatively well-characterized with evidence for sedimentary and igneous components from the slab variably contributing to mantle sources across the arc (Patino et al., 2000). It is a "warm" subduction zone, with predicted slab interface temperatures of ~800 °C at 100 km depth beneath Costa Rica (Peacock et al., 2005), resulting in sporadic slab melting (Hoernle et al., 2008). Thus, it may be considered an analog for subduction zones at a time when subduction temperature gradients were steeper. In Central America, metamorphic rocks cannot be used to constrain net subduction fluxes because no section of metasediments having undergone the subduction P-T pathway is known to occur in the geological record. Instead, net subduction fluxes of volatiles are estimated from comparing their concentrations and isotopic compositions in the offshore altered oceanic crust (Li and Bebout, 2005; Busigny et al., 2019) with their concentrations and isotopic compositions in arc fumaroles that represent volcanic outgassing fluxes. This mass balance calculation can be hampered by ubiquitous infiltration of air into most fumaroles, as evidenced by noble gases systematics: although fumaroles typically show mantle-like helium isotope ratios, neon and argon budgets are overwhelmed by atmospheric components (Hilton et al., 2002; Snyder et al., 2003). This is also a problem for nitrogen. Historically, SO_2/N_2 ratios from fumaroles and the overall SO_2 outgassing flux have been used to determine a total N_2 volcanic outgassing flux for the central American arc, yielding a value of 1.7×10^9 mol N_2/yr, or 3.4×10^9 mol N/yr (Hilton et al., 2002; Fischer et al., 2002). This is comparable to an estimate of the central American subduction nitrogen flux of $\sim 1.1 \times 10^9$ mol N/yr (equivalent to $\sim 5.7 \times 10^8$ mol N_2/yr) from Busigny et al. (2019). These flux estimates are given with no uncertainties, but they appear comparable within a factor of 2. Taken at face value, this would support inefficient N recycling from the surface to the deep mantle. However, fumaroles incorporate air-derived N_2, after the infiltration of meteoric water within subsurface hydrothermal systems and/or because of sampling techniques (Fischer et al., 2002). Thus, the outgassing N_2 fluxes based on raw N_2/SO_2 ratios in fumaroles are overestimates of the outgassing N_2 flux. As a remedy, the volcanic fraction of N_2 in fumaroles was quantified on the basis of N_2/Ar ratios: air-saturated waters have a known N_2/Ar ratio of ~40 at STP but most hydrothermal gases in the CAVA have ratios >80 (Hilton et al., 2002; Fischer et al., 2002; Elkins et al., 2006; Snyder et al., 2003; Zimmer et al., 2004). The N_2 amount in excess of air-saturated water, termed N_2^*, was suggested to reflect the volcanic N_2 fraction (Hilton et al., 2002; Fischer et al., 2002). A volcanic nitrogen degassing flux of 2.9×10^8 mol N_2/yr was estimated for the central American arc (Fischer et al., 2002). This degassing flux estimate is lower by a factor of 2 than the subduction nitrogen flux of $\sim 5.7 \times 10^8$ mol N_2/yr (or $\sim 1.1 \times 10^9$ mol N/yr), suggesting N_2 sequestration into the deep mantle by subduction, even in a warm subduction zone (Busigny et al., 2019; Li and Bebout, 2005).

Here, we take a new approach to constrain the origin of N_2 as well as light noble gases in CAVA fumaroles and springs. We use the newly-developed $^{15}N^{15}N$ tracer of atmospheric contamination (Labidi et al., 2020; Yeung et al., 2017; Young et al., 2016). Specifically, we use Δ_{30}, the $^{15}N^{15}N$ concentration relative to a random distribution of ^{14}N and ^{15}N atoms among N_2 molecules, as a tracer of surficial atmospheric contamination. The Δ_{30} tracer is defined as $\Delta_{30} = {}^{30}R/({}^{15}R)^2 - 1$ (‰), where ${}^{30}R = {}^{15}N^{15}N/{}^{14}N^{14}N$ and ${}^{15}R = {}^{15}N/{}^{14}N$ for the gas of interest. At relevant temperatures ranging from 200 to 1000 °C, equilibrium among N_2 isotopologues results in Δ_{30} values from 0.5 to 0.1‰, respectively (Yeung et al., 2017). This applies for any magmatic and crustal N_2, whether it is mantle-derived, inherited from the slab, or shallow crustal reservoirs (Labidi et al., 2020). In contrast, air has a pronounced disequilibrium $^{15}N^{15}N$ enrichment, leading to an atmospheric Δ_{30} value of 19.1 ± 0.3‰ (2σ) (Yeung et al., 2017). We make use of this disequilibrium as a tracer for air contributions in natural fluids and identify the compositions of mantle sources for N_2 and light noble gases for 15 fumaroles and gases bubbling from springs in Costa Rica, Panama, Nicaragua, and El Salvador. Our $^{15}N^{15}N$ data allows determination of the $N_2/^3He$, $^3He/^{36}Ar$ and $^3He/^{22}Ne$ ratios for the CAVA mantle sources. Using an updated ^3He outgassing flux for the region, we provide a new range of estimates for the N_2 outgassing flux along the Central American arc. Our result has implications for the net subduction flux of nitrogen, suggesting that the net sequestration of nitrogen to the mantle is within error of zero.

2. Geological context and samples

The CAVA results from the eastward subduction of the Cocos Plate beneath the Caribbean Plate. Abundant literature describes the spectrum of sub-arc mantle sources, incorporating slab sedimentary components beneath Nicaragua, to volcanic seamounts derived from Galapagos underneath Costa Rica and Panama (Carr et al., 2003; Gazel et al., 2009; Hoernle et al., 2008; Patino et al., 2000; Ranero and von Huene, 2000; Schwarzenbach et al., 2016).

Eight gas samples from fumaroles were collected from Poás and Momotombo volcanoes during several field expeditions in the early to mid-2000's with gas chemistry and isotope data published in Zimmer et al. (2004), Elkins et al. (2006), De Leeuw et al. (2007) and Fischer et al. (2015). Fumaroles had outlet temperatures ranging from 98 °C to 747 °C. Samples were collected in pre-evacuated Giggenbach bottles filled with 5N NaOH solution (Giggenbach, 1992). Gas splits were taken from the headspace of the bottles with sealed glass tubes shortly after sample collection and stored until analyzed for this work. Five gases from the Poás crater were collected between 2003 and 2006, from the fumarolic sites "Official" and "Naranja", at temperatures between 98 °C and 158 °C. For these, we report new N_2 isotopologue and $^{40}Ar/^{36}Ar$ data. $^3He/^4He$ of these samples are 7.0 ± 0.2 R_A (Hilton et al., 2010) where R_A is air $^3He/^4He$ or 1.384×10^{-6}. Gas chemistry is available from previous work (Fischer et al., 2015). One fumarole sample was collected at Santa Ana Volcano (Salvador), with a vent temperature of 400 °C. It has a helium isotope ratio of 7.5 ± 0.1 R_A (De Leeuw et al., 2007). The He-Ne-Ar abundances are known (De Leeuw et al., 2007). No $^{40}Ar/^{36}Ar$ is available but other gases from El Salvador all have near-atmospheric $^{40}Ar/^{36}Ar$ ratios (Snyder et al., 2003). We additionally discuss two fumarole gas samples collected at Momotombo in Nicaragua, at an outlet temperature of ~750 °C. For these two samples, we report new $^{40}Ar/^{36}Ar$ isotope measurements. N_2 isotopologues, helium isotopes, He-Ne-Ar and major gas chemistry data for these samples are available from previous work (Elkins et al., 2006; Yeung et al., 2017). Hot springs found in the flanks of volcanic arcs are the most accessible samples, and hence are routinely used to characterize volcanic end-members (e.g. Snyder et al., 2003). As a means to compare these to our fumaroles, we also report data from seven gases from bubbling springs in Costa Rica and Panama, collected in 2018 as part of the *Biology Meets Subduction* initiative. Sample collection sites are shown on Fig. 1. Samples were collected in 15 cm^3 copper tubes following standard procedures. Waters in the springs had temperatures between 29 °C and 55 °C. For these, we report major element gas compositions, N_2 isotopologues and He–Ne–Ar systematic data.

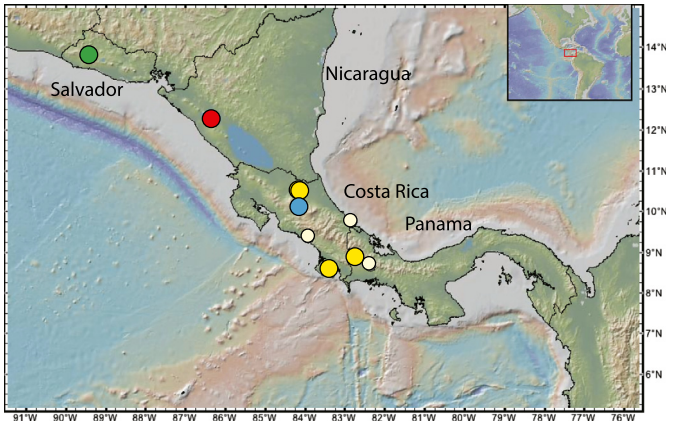

Fig. 1. Location of all the samples studied here. Green, red and blue symbols are fumarole locations from Santa Ana, Momotombo and Poás (Data in Table 1). Yellow symbols are springs (Data in Table 2). (For interpretation of the colors in the figure(s), the reader is referred to the web version of this article.)

3. Methods

Gas aliquots were split up to three ways and processed for (1) gas chemistry, (2) N_2, and (3) noble gases systematics. Inorganic gas components (such as N_2, He, Ar and O_2) and methane were separated and quantified on a TCD gas chromatograph coupled with a quadrupole mass spectrometer as in earlier work (Fischer et al., 2015). This allowed determining the N_2/He and N_2/Ar ratios of each gas splits. Nitrogen isotopologues were determined via high-resolution mass spectrometry at the University of California, Los Angeles (Young et al., 2016). Noble gas analyses were conducted at the University of Oxford (UK) and at the University of New Mexico using standard methods (Barry et al., 2016; Lee et al., 2017). Details may be found in the supplementary online file.

4. Results

We present an integrated dataset that includes concentrations of He, Ne, Ar, N_2, O_2, and CH_4, elemental ratios of those gases, noble gas isotope compositions, and N_2 isotopologue ratios. Data for the fumaroles (n = 8) are in Table 1 and data for the springs (n = 7) are in Table 2.

4.1. $\delta^{15}N$ and Δ_{30} relationships

Newly determined Δ_{30} values vary between 19.3 ± 0.4‰ and 3.5 ± 1.0‰ (1σ uncertainty, Fig. 2). Two previously published data points from Momotombo extend the range down to 1.5 ± 0.6‰ and are plotted on Fig. 2 (Yeung et al., 2017). The highest Δ_{30} is similar to the air value of 19.1 ± 0.3‰ (2σ). The range in Δ_{30} values suggests samples incorporate variable amounts of atmospheric nitrogen, contributing between ~8 and ~100% of the total N_2. Fumaroles from Poás and Momotombo have the lowest Δ_{30} values, indicating that these fumaroles have the lowest air-derived N_2 contributions. A range of $\delta^{15}N$ values is observed, with values of between -3.7 ± 0.3‰ and $+4.2 \pm 0.3$‰ (Fig. 2). For Poás and Momotombo, $\delta^{15}N$ values are $+0.4 \pm 0.3$‰ and $+5.4 \pm 0.3$‰ respectively, where air contributions are at their lowest values (minimum Δ_{30}). The $\delta^{15}N$ values as a whole (with both low and high Δ_{30}) are within the range of $\delta^{15}N$ values of between -3.0 ± 0.6 and 6.3 ± 0.3‰ (n = 73) reported previously for central American gases (Elkins et al., 2006; Fischer et al., 2015, 2002; Snyder et al., 2003; Zimmer et al., 2004). The $\delta^{15}N$ values exhibit a negative correlation with Δ_{30} values (Fig. 2).

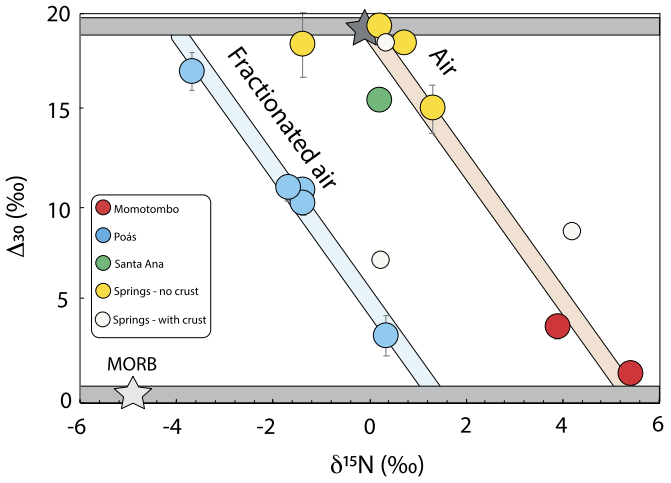

Fig. 2. The nitrogen isotopic composition of volcanic discharges in central America. Variable Δ_{30} values establish that our samples incorporate variable amounts of atmospheric nitrogen. Fumaroles from the Poás and Momotombo have the lowest Δ_{30} values indicating they have the lowest air-derived N_2 contributions while the hot springs from Costa Rica have the highest air contributions. Variable $\delta^{15}N$ values are observed, between -3.7 ± 0.3‰ and $+4.2 \pm 0.3$‰. At an air Δ_{30} values, variable $\delta^{15}N$ must be caused by a mass-dependent isotope fractionation, presumably associated with hydrothermal degassing. The high-temperature components have positive $\delta^{15}N$ values.

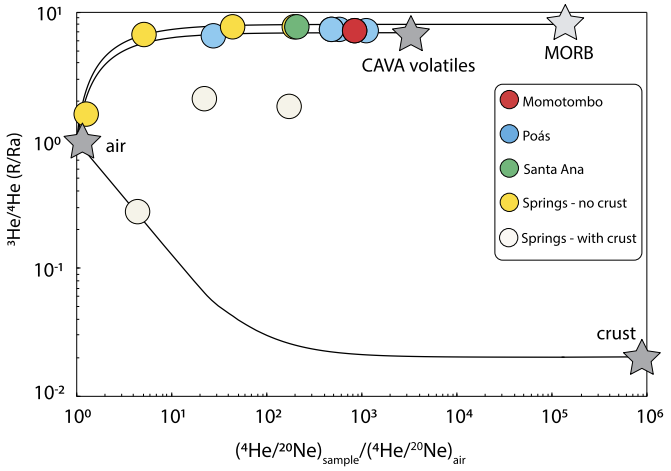

Fig. 3. Measured $^3He/^4He$ ratios versus $^4He/^{20}Ne$ ratios of the samples, normalized to air by convention (De Leeuw et al., 2007). Most samples indicate simple two-component air-magma mixing. Three Costa Rica hot springs (HS) however show additions of crustal ^4He.

4.2. Noble gas isotopes

Concentrations of He, Ne and Ar vary over 4 orders of magnitude and are correlated (Table 1 and 2). We observe $^{40}Ar/^{36}Ar$ ratios between 297 ± 5 and 342 ± 5 for our samples (Table 1 and 2), far from the upper mantle value of ~25,000 (Moreira et al., 1998) but close to air at 298.5 (Lee et al., 2006). This is comparable to the known range of values for Central American rocks and gases of between 292 ± 7 and 310 ± 5 (Fischer et al., 2005; Kennedy et al., 1991; Snyder et al., 2003; Staudacher and Allègre, 1988). The $^{20}Ne/^{22}Ne$ and $^{21}Ne/^{22}Ne$ ratios are known only for the hot springs, and data appear indistinguishable from air (Table 2).

The $^3He/^4He$ ratios vary substantially, between 0.3 and 7.6 ± 0.1 R_A. Unlike Ne and Ar, the He budget is not significantly affected by atmospheric components and instead reflects appreciable deep contributions. The $^3He/^4He$ ratios are broadly correlated with $^4He/^{20}Ne$ ratios (Fig. 3). Most of the data are explained by two-component mixing between air ($^3He/^4He$ = 1 R_A by definition,

Table 1
Nitrogen and light noble gases isotope and concentrations for central Americans fumaroles.

		PO 06-1-3	PO 03-2	Pnar06-1	PO 06-1-1	PO 06-1-2	ES02 10	Nic-3	Nic-2
dates of collection		Poas 11/5/06	Poas 3/31/03	Poas 2/24/06	Poas 2/24/06	Poas 2/24/06	Santa Ana	Momotombo 1/5/02	Momotombo 1/5/02
latitude		10.12	10.12	10.12	10.12	10.12	13.5111	12.2519	12.2519
longitude		−84.1359	−84.1359	−84.1359	−84.1359	−84.1359	−89.3748	−86.3224	−86.3224
temperature (°C)		113	98	153	113	113	400	747	747
quantity of processed N_2	10^{-6} mol	2.1	2.2	8.8	8.0	5.8	22.4		
N_2 vol fraction (ucla)	$\times 10^{-2}$	9.21E-01	8.47E-01	3.10E-01	7.43E-01	6.01E-01	7.14E-01		
$\delta^{15}N$	vs. air	−3.69	0.35	−1.38	−1.38	−1.7	0.2	5.41	3.89
Δ_{30}	vs. stochastic	17	3.43	10.92	10.25	11	15.5	1.5	3.9
1 se $\delta^{15}N$		0.032	0.018	0.02	0.021	0.022	0.008	0.1	0.1
1 se Δ_{30}		0.496	0.527	0.288	0.309	0.307	0.138	0.3	0.2
CO_2		0.992	0.990	0.975	0.993	0.990	0.983	0.859	0.861
He		4.56E-05	5.00E-06	5.59E-06	4.97E-06	8.53E-06	6.54E-06	7.61E-06	1.66E-05
H_2		1.17E-04	3.25E-04	1.40E-02	6.62E-05	7.05E-05	4.64E-03	1.24E-01	1.20E-01
Ar		2.42E-04	1.12E-04	1.24E-04	3.10E-04	4.21E-04	9.98E-05	1.52E-04	3.70E-05
O_2		4.19E-04	1.25E-05	1.45E-04	5.28E-04	7.90E-04	4.54E-06	1.14E-05	8.93E-06
N_2		6.70E-03	1.00E-02	1.06E-02	6.56E-03	8.94E-03	1.20E-02	1.62E-02	1.88E-02
CH_4		6.44E-06	1.25E-06	1.20E-04	7.24E-06	9.48E-06	1.95E-05	8.88E-06	7.66E-06
He/Ar		1.89E-01	4.44E-02	4.50E-02	1.60E-02	2.03E-02	6.55E-02	5.00E-02	4.48E-01
N_2/He		1.47E+02	2.00E+03	1.91E+03	1.32E+03	1.05E+03	1.83E+03	2.13E+03	1.13E+03
N_2/Ar		2.77E+01	8.89E+01	8.58E+01	2.11E+01	2.12E+01	1.20E+02	1.07E+02	5.07E+02
O_2/N_2		6.25E-02	1.25E-03	1.36E-02	8.04E-02	8.83E-02	3.80E-04	7.03E-04	4.76E-04
N_2/CH_4		1.04E+03	8.00E+03	8.87E+01	9.06E+02	9.43E+02	6.14E+02	1.83E+03	2.45E+03
$^{40}Ar/^{36}Ar$					297	293		305	
$^3He/^4He$	(Ra)	6.44	7.15	6.96	7.15	7.15	7.56	6.99	6.99
$N_2/^3He$		1.63E+07	2.00E+08	1.96E+08	1.32E+08	1.05E+08	1.73E+08	2.18E+08	1.16E+08
$N_2/^{36}Ar$		8.49E+03	2.72E+04	2.62E+04	6.47E+03	6.49E+03		3.26E+04	1.78E+05
$^4He/^{20}Ne$		8.93E+00	1.90E+02	3.61E+02	1.56E+02	1.56E+02	6.66E+01	2.75E+02	2.75E+02
$^3He/^{22}Ne$		8.04E-04	1.90E-02	3.52E-02	1.56E-02	1.56E-02	7.05E-03	2.69E-02	2.69E-02
X value		28	596	1133	488	488	209	864	864
$^{22}Ne/^{36}Ar$		6.47E-01	7.16E-03	3.81E-03	3.15E-03	3.98E-03		5.55E-03	
$^3He/^{36}Ar$		5.20E-04	1.36E-04	1.34E-04	4.90E-05	6.20E-05		1.50E-04	
$^4He/^{40}Ar$		1.89E-01	4.46E-02	4.51E-02	1.61E-02	2.03E-02		5.02E-02	

$^4He/^{20}Ne = 0.3188$) and a magmatic endmember. The magmatic component has a $^3He/^4He$ of ∼7 (Fig. 3). The $^4He/^{20}Ne$ ratio of the magmatic component must be at least as high as the highest value from our dataset, ∼270. Three Costa Rican springs show a clear offset from the two-component mixing line, showing much lower $^3He/^4He$ ratios at a given $^4He/^{20}Ne$ value. Similar features in other Central American gases were interpreted to result from mixing with gases from crustal fluids (De Leeuw et al., 2007).

4.3. Nitrogen, oxygen and methane concentrations

Nitrogen concentrations vary from 0.2 vol% to 93 vol% in the springs, and from 0.6 vol% to 1.9 vol% in the fumaroles (Table 1 and 2). Oxygen concentrations are variable, resulting in O_2/N_2 ratios ranging over two orders of magnitude, between 3.8×10^{-4} to 1.1×10^{-1} (Supplementary Fig. 1). The O_2/N_2 ratios are not directly correlated with Δ_{30} values (supplementary Fig. 1), suggesting that O_2/N_2 is not a reliable indicator of the presence of nitrogen from air. Methane concentrations are below 0.1 vol% for most samples, with the exception of two of the Costa Rica hot springs, where CH_4 concentrations are as high as ∼80 vol%, suggesting contributions from shallow crustal gases (Snyder et al., 2003). N_2/CH_4 varies over 5 orders of magnitude, between $\sim 1.2 \times 10^{-1}$ to $\sim 2.1 \times 10^4$, but remains uncorrelated with Δ_{30} values (Supplementary Fig. 1).

4.4. Nitrogen - noble gas ratios

We compute N_2/Ar, $N_2/^{36}Ar$, N_2/He and $N_2/^3He$ ratios, with a ±20% relative uncertainty on individual samples. N_2/Ar ratios are between 21 and 120 for most samples, with one sample from Momotombo at 507 (Fig. 4). For comparison, the air value is ∼84, air-saturated water (ASW) at STP is ∼41, and MORB gases have N_2/Ar ratios of 55 ± 5 (Javoy and Pineau, 1991), although a higher estimate of $\sim 120 \pm 40$ (Marty and Dauphas, 2003) was derived from MORB samples with unusually radiogenic $^{40}Ar/^{36}Ar$ ratios (data from Marty and Zimmermann, 1999). For samples where $^{40}Ar/^{36}Ar$ was measured, $N_2/^{36}Ar$ ratios vary between 1.2×10^4 and 4.2×10^4. Assuming the $^{40}Ar/^{36}Ar$ is atmospheric as for other Central American gas samples (Snyder et al., 2003), the $N_2/^{36}Ar$ range extends to between 6.5×10^3 and 1.5×10^5 (Fig. 4). This includes values below and above both air (2.5×10^4) and air-saturated water at STP (1.3×10^4). The highest $N_2/^{36}Ar$ value remains well below estimates of the convective mantle of $\sim 2 \times 10^6$ (Labidi et al., 2020; Marty and Humbert, 1997) even for samples where Δ_{30} is low.

The N_2/He ratios vary between 1.5×10^2 and 4.2×10^4, below the value of air of 1.5×10^5 or air-saturated water $\sim 3.0 \times 10^5$ (Fig. 5). Similarly, $N_2/^3He$ ratios vary between 1.6×10^7 and 1.1×10^{11} (Fig. 5), mostly below the value of air and ASW of 1.0×10^{11} and $\sim 2.0 \times 10^{11}$ respectively (Ballentine et al., 2002). The N_2/He (and $N_2/^3He$ ratios) are correlated with Δ_{30} values and are described by two-component mixing hyperbolae between air (or air-saturated waters) and high-temperature components with elevated N_2/He (and $N_2/^3He$ ratios) relative to MORB gases (Fig. 5).

4.5. Noble gas ratios

The $^3He/^{22}Ne$ ratios range over 4 orders of magnitude, between 8.9×10^{-6} and 2.7×10^{-2} (Fig. 6). These values are between air, at 4.5×10^{-6}, and upper-mantle gases at $\sim 5.5 \times 10^1$ (Moreira et al., 1998). The $^4He/^{20}Ne$ ratios are also ranging between air and the upper-mantle value (Supplementary Figure 2). $^3He/^{22}Ne$

Table 2
Nitrogen and light noble gases isotope and concentrations for central American springs.

sample ID		LH180406	PX180416	PS180405	BS180407	HA180403	CW180415	XF180416
spring name		Los Pozos	San Juan PraxAir	Playa Sandalo	Bajo Mended	Hatillo	Cauhita	San Juan PraxAir
latitude		8.870954	10.488755	8.575544	8.66645	9.360224	9.735746	10.485523
longitude		−82.689901	−84.113598	−83.36416	−82.349098	−83.916639	−82.825737	−84.113229
temperature (°C)		55	29	31	41	33	35	29
quantity of processed N_2	10^{-6} mol	18.0	38.0	28.0	588.0	556.0	39.2	2.8
N_2 vol fraction (ucla)	$\times 10^{-2}$	2.89E-02	6.10E-02	4.49E-02	9.44E-01	8.92E-01	6.29E-02	4.49E-03
$\delta^{15}N$	vs. air	−1.38	0.20	0.71	4.19	0.22	0.34	1.30
Δ_{30}	vs. stochastic	18.39	19.35	18.42	8.73	7.29	18.47	15.09
1 se $\delta^{15}N$		0.029	0.007	0.008	0.004	0.004	0.004	0.031
1 se Δ_{30}		0.825	0.22	0.24	0.168	0.077	0.097	0.617
CO_2		0.997	0.944	0.082		0.031	0.054	
He		1.47E-07	1.97E-06	1.90E-06		4.19E-04	1.04E-05	
H_2		9.07E-07	9.81E-08	1.51E-05		7.48E-05	1.62E-05	
Ar		4.79E-05	3.52E-04	1.07E-03		6.90E-03	1.71E-03	
O_2		5.75E-04	1.19E-02	2.77E-03		3.12E-02	1.10E-02	
N		2.04E-03	4.41E-02	5.03E-02		9.30E-01	9.92E-02	
CH_4		9.62E-08	2.66E-06	8.64E-01		3.09E-04	8.34E-01	
He/Ar		3.07E-03	5.60E-03	1.77E-03	2.57E-03	6.07E-02	6.09E-03	3.85E-02
N_2/He		1.39E+04	2.23E+04	2.65E+04	4.23E+04	2.22E+03	9.56E+03	1.21E+03
N_2/Ar		4.27E+01	1.25E+02	4.69E+01	1.09E+02	1.35E+02	4.64E+01	4.64E+01
O_2/N_2		2.81E-01	2.69E-01	5.50E-02		3.36E-02	1.11E-01	
N_2/CH_4		2.12E+04	1.65E+04	5.82E-02		3.01E+03	1.19E-01	
^{4}He	$\times 10^{-9}$ cc/ccSTP	3.21E+01	1.12E+03	1.65E+02	2.23E+04	3.98E+05	4.40E+03	3.72E+03
^{20}Ne	$\times 10^{-9}$ cc/ccSTP	2.24E+00	6.81E+02	3.98E+02	1.58E+04	7.07E+03	6.15E+02	5.85E+01
^{40}Ar	$\times 10^{-6}$ cc/ccSTP	3.85E+00	3.95E+02	4.83E+02	8.67E+03	6.35E+03	7.49E+02	9.65E+01
^{36}Ar	$\times 10^{-9}$ cc/ccSTP	1.28E+01	1.29E+03	1.59E+03	2.67E+04	2.06E+04	2.43E+03	3.16E+02
^{40}Ar/^{36}Ar		301	305	304	325	308	309	306
^{3}He/^{4}He	(R_A)	7.48	6.52	1.55	0.27	1.82	2.05	7.59
^{20}Ne/^{22}Ne		10.00	9.82	9.84		9.85	9.87	9.91
^{21}Ne/^{22}Ne		0.023	0.029	0.029		0.029	0.029	0.029
$N_2/^3$He		1.33E+09	2.45E+09	1.22E+10	1.12E+11	8.72E+08	3.33E+09	1.14E+08
$N_2/^{36}$Ar		1.29E+04	3.83E+04	1.43E+04	3.53E+04	4.17E+04	1.80E+04	1.42E+04
^{4}He/^{20}Ne		1.43E+01	1.65E+00	4.15E-01	1.41E+00	5.63E+01	7.15E+00	6.37E+01
^{3}He/^{22}Ne		1.50E-03	1.48E-04	8.85E-06	5.34E-06	1.41E-03	2.02E-04	6.70E-03
X value		45	5	1	4	177	22	200
^{22}Ne/^{36}Ar		6.49E-03	1.06E-01	1.32E-01		3.39E-02		5.00E-02
^{3}He/^{36}Ar		9.70E-06	1.57E-05	1.17E-06	3.16E-07	4.78E-05	5.41E-06	1.25E-04
^{4}He/^{40}Ar		3.08E-03	5.62E-03	1.77E-03	2.50E-03	6.09E-02	6.11E-03	

(and ^{4}He/^{20}Ne) ratios are correlated with Δ_{30} values (Fig. 6, Supp. Fig. 2). At $\Delta_{30} = 0$ the high-temperature component appears to have He/Ne ratios lower than MORB gases by about four orders of magnitude (Fig. 6, Supp. Fig. 2). The ^{3}He/^{36}Ar ratio ranges between 1.6×10^{-6} and 1.7×10^{-4} (Fig. 6). This is higher than the air value of 2.5×10^{-7}, but considerably lower than the upper-mantle value of $\sim 5.0 \times 10^{-1}$ (Moreira et al., 1998; Raquin et al., 2008). A similar observation can be made of the ^{4}He/^{40}Ar ratio (Supp. Fig. 2). The variations in ^{3}He/^{36}Ar (and ^{4}He/^{40}Ar) ratios are correlated with Δ_{30} values and at $\Delta_{30} = 0$, the high-T component shows ^{3}He/^{36}Ar ratios lower than MORB gases by about three orders of magnitude (Fig. 6, Supp. Fig. 2). Most ^{22}Ne/^{36}Ar ratios in fumaroles and springs range between 1.3×10^{-1} and 3.1×10^{-3} (with one outlier at $\sim 6.5 \times 10^{-1}$, the Poás gas with the Δ_{30} value closest to air). The higher values are similar to the air and MORB values of 5.0×10^{-2} and 1.0×10^{-1}, respectively (Mukhopadhyay, 2012) and are observed for samples with air-like Δ_{30} values. At $\Delta_{30} = 0$, much lower ^{22}Ne/^{36}Ar values are observed, lower than both MORB and air by one to two orders of magnitude (Table 1 and 2).

5. Discussion

Our rationale is that correlations between Δ_{30} and various isotope and element ratios can be used to identify and correct for air components and reveal pristine high-temperature endmembers. Air is identified with a Δ_{30} of 19.1 ± 0.3‰, while any N_2 produced by a geologic process such as magmatic degassing has $\Delta_{30} \sim 0$‰ (Labidi et al., 2020). Arguments against re-ordering and crustal contamination are given in the supplementary discussion.

5.1. Atmospheric N_2 may easily go unnoticed

CAVA gas Δ_{30} values are variable, indicating commensurately variable contributions of air to the N_2 budgets in hydrothermal discharges. Based on Δ_{30} data, air accounts for 40 to 100% of the N_2 in the springs. In fumaroles, air accounts for 8 to 90% of the N_2. Atmospheric N_2 is therefore ubiquitous. Systematics involving $\delta^{15}N$, [O_2], O_2/N_2, N_2/He and N_2/Ar ratios may disentangle magmatic N_2 from air-derived N_2 in gas discharges (Sano et al., 2001; Fischer et al., 2002; Elkins et al., 2006). The rationale for all of those approaches is that air has known $\delta^{15}N$, O_2/N_2, N_2/He and N_2/Ar ratios, that are different from magmatic components. Our Δ_{30} data present a series of challenges to these previous approaches. For example, samples with high ^{4}He/^{20}Ne ratios were suggested to illustrate a volatile budget largely uncontaminated by air, especially when a number of other criteria are met, e.g., O_2/N_2 ratios $<10^{-3}$, high outlet temperatures, or non-atmospheric N_2/Ar ratios (Elkins et al., 2006). The Santa Ana volcano fumarole is vented at 400 °C, a ^{4}He/^{20}Ne ~200 times higher than air and a O_2/N_2 ratio of $\sim 10^{-4}$ (Table 1, Fig. 3), which would suggest minimal air contamination. However, the near-air Δ_{30} of 15.5 ± 0.3‰ requires that ~80% of N_2 is from air in this sample, showing that high ^{4}He/^{20}Ne, even in conjunction with high vent temperature and low O_2/N_2, is

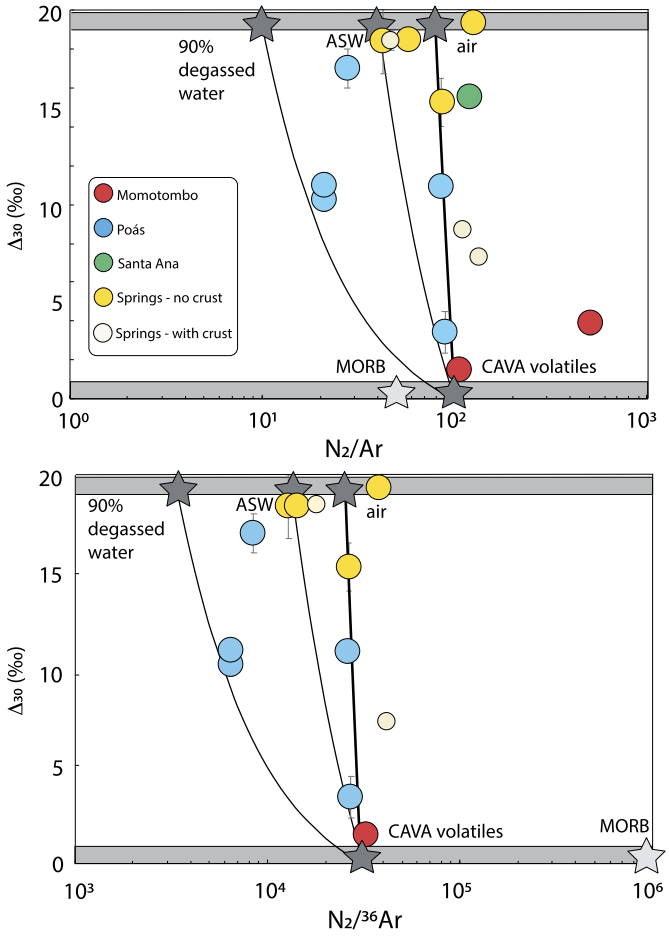

Fig. 4. Measured N_2/Ar and $N_2/^{36}$Ar ratios versus Δ_{30} values. Mixing lines are shown for mixtures between the high-temperature component observed at both Momotombo and Poás, and variably fractionated atmospheric components, including air, air-saturated water (ASW), and degassed water. The high-temperature endmembers with $\Delta_{30} = 0‰$ defined by the data from Momotombo and Poás have similar N_2/Ar and $N_2/^{36}$Ar ratios of ~100 and ~10^4, respectively. Here, we adopt values of ~100 and 3×10^4 for N_2/Ar and $N_2/^{36}$Ar ratios for the high-T endmember at Momotombo. Nitrogen and argon have indistinguishable solubilities in silicate melts and thus are not fractionated by magmatic degassing at ~1200 °C (Libourel et al., 2003). Thus, the low $N_2/^{36}$Ar at Momotombo is not resulting from fractionations during magmatic degassing. Instead, it may be a feature of the Momotombo mantle source. At Poás, fumarole samples are consistent with the same N_2/Ar ratio for the high-temperature component as at Momotombo. If hydrothermal degassing affected the high-T volatiles at Poás, the pristine N_2/Ar and $N_2/^{36}$Ar for high-T gases at Poás could be higher than the observed values. Note that combining a ^{3}He/^{36}Ar ratio of ~10^{-4} (see Fig. 6B) to the observed $N_2/^3$He of ~10^8 (Fig. 4) returns to a $N_2/^{36}$Ar of ~10^4, consistent with the conclusion of a low N_2/Ar in our sampling of high-temperature endmembers (see section 5.4).

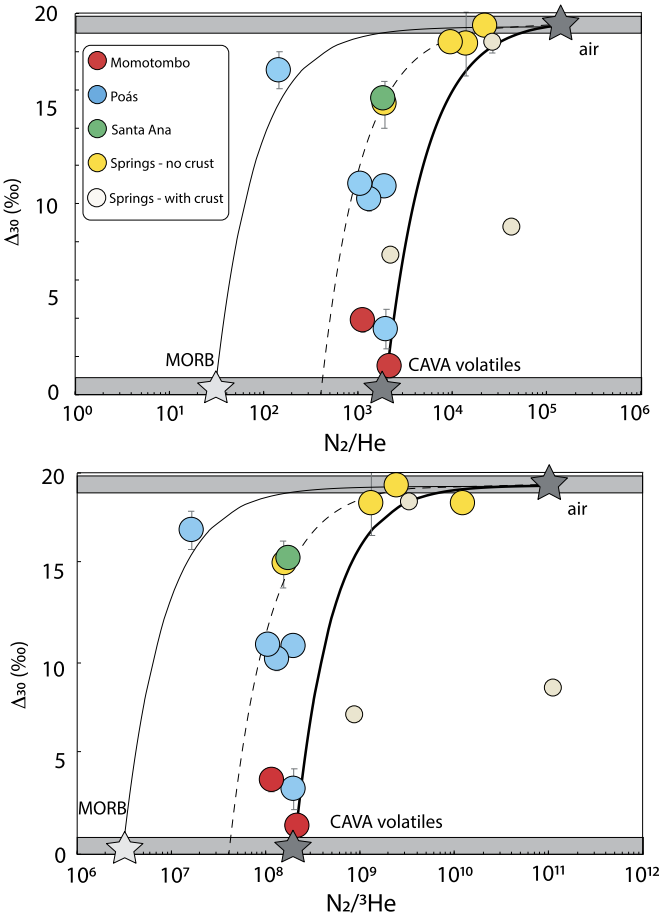

Fig. 5. Measured N_2/He and $N_2/^3$He ratios versus Δ_{30} values. Mixing lines are shown for mixtures between air and three high-temperature components: MORBs, and two variably N_2-enriched endmembers required to fit the data. Springs with additions of crustal ^{4}He are shown in the smallest symbols. They are not used for fluxes calculations – see discussion in the supplementary discussion.

not necessarily sufficient evidence that N_2 is dominantly magmatic (See supplementary discussion).

5.2. Atmospheric N_2 undergoes isotopic fractionation in hydrothermal systems

Nitrogen isotope ratios could be a direct tracer of atmospheric N_2, since air and magma-derived nitrogen are thought to have distinct δ^{15}N values (Fischer et al., 2002; Sano et al., 2001). The Δ_{30} data confirm the veracity of this approach for most, but not all, samples. Gases (except those from Poás) fall on a single two-component mixing trend between air and a high-temperature component with near-zero Δ_{30} and δ^{15}N of ~5‰ (Fig. 2). For those, the air component appears unfractionated with respect to δ^{15}N. When mixed with high-temperature volatiles, δ^{15}N increases and Δ_{30} values decrease (Fig. 2).

Samples from Poás are different. They form a unique linear mixing trend where both air-derived and high-temperature N_2 are distinct from elsewhere in the arc system, with δ^{15}N endmember values of $-4.0 \pm 0.3‰$ and $+1.0 \pm 0.3‰$ for air and the high-T component, respectively (Fig. 2). This represents a ~4‰ shift for both endmembers compared to values observed elsewhere on the arc. Our observation creates ambiguities at Poás, since there, and there only: (1) high-temperature δ^{15}N is only marginally higher than air; and (2) air-derived N_2 has a δ^{15}N very similar to the MORB value of $-5 \pm 2‰$ (Javoy and Pineau, 1991; Marty and Zimmermann, 1999).

The data from Poás require that atmospheric N_2 experienced a ~4‰ mass-dependent ^{15}N/^{14}N fractionation in the sub-surface. This may result from the degassing of once air-saturated waters. The isotopic fractionation associated with N_2 dissolved in water was experimentally documented to be +0.9 to −0.4‰ from 6 to 60 °C (Lee et al., 2015). The dissolved-gas isotope fractionation was shown to cross over at about 40 °C, from a positive to a negative sign (Lee et al., 2015). Above 40 °C, the isotopic difference between dissolved and gaseous N_2 increases: isotopically light N_2 is increasingly partitioned in the dissolved fraction as temperature increases. This behavior indicates that a kinetic isotope effect attends N_2 dissolution/degassing in geothermal waters (Lee et al., 2015). Using the experimental results of Lee et al. (2015), we calculate the consequences of N isotope fractionation during open-system degassing using Rayleigh fractionation. At 60 °C, with a gas/dissolved-gas ^{15}N/^{14}N fractionation factor of 1.0004, the lowest δ^{15}N values of

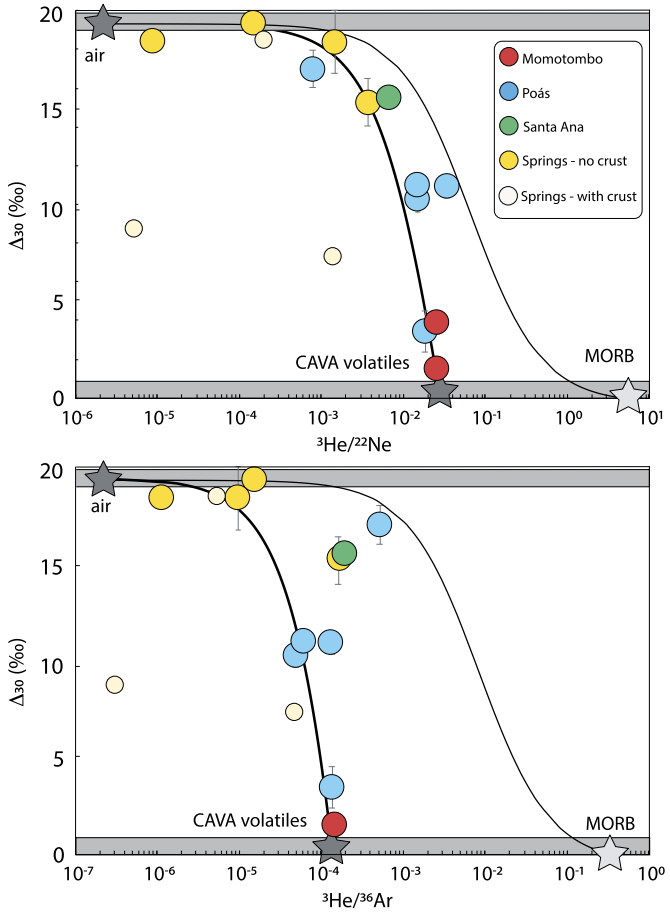

Fig. 6. Measured $^{3}He/^{22}Ne$ and $^{3}He/^{36}Ar$ ratios versus Δ_{30} values. Springs with additions of crustal ^{4}He are shown in the smallest symbols. They are not used for fluxes calculations – see discussion in the supplementary discussion. Mixing lines are the same as in Fig. 3 and 4. They are shown for mixtures between air and high-temperature components: MORB, and a N_2-^{36}Ar-^{22}Ne enriched endmember that fits the data. The mixing relationships are curved because of the logarithm scale, but also because of how distinct the N_2/Ne of the mixing endmembers may be. Air has a $N_2/^{20}Ne$ ratio of air is 4.5×10^4. We calculate a $N_2/^{20}Ne$ of 1.3×10^6. This is based on a $N_2/^{3}He$ of 3×10^6 for the MORB mantle (Javoy and Pineau, 1991). We combine this $N_2/^{3}He$ estimate with $^{3}He/^{4}He$ and $^{4}He/^{20}Ne$ values for the MORB mantle from Moreira et al. (1998). Using the $^{3}He/^{22}Ne$ ratio of the MORB mantle (Moreira et al., 1998), we derive a $N_2/^{22}Ne$ of 1.7×10^7. Conversely, we here derive $N_2/^{3}He$, $^{3}He/^{22}Ne$ ratios of the central American high-temperature volatiles. Combining those with $^{3}He/^{4}He$ of ~7 from Fig. 3, we derive $N_2/^{20}Ne$ and $N_2/^{22}Ne$ ratios of 3.4×10^5 and 3.3×10^6, respectively. On panel b, the curvatures are function the N_2/Ar of the mixing endmembers, which are estimated on Fig. 4.

~−3.5‰ with air-like Δ_{30} require that the N_2 sampled by the fumaroles is the residuum left over after degassing of about 99.98% of the dissolved nitrogen. Extrapolating the temperature dependence of the fractionation factor to 100 °C, 97% degassing of N_2 is required to account for a $\delta^{15}N$ of ~−3.5‰.

We envision the hydrothermal degassing to be the natural consequence of hydrothermal systems experiencing continuous degassing in the absence of continuous meteoric (air-saturated) water recharge. It is puzzling however that among the sites we sampled, air nitrogen undergoes isotopic fractionation only at Poás. In order to explain this observation, we suggest a restricted set of conditions is met in the Poás subsurface, but not elsewhere. Gases from Momotombo and Santa Ana are vented at temperatures between 747 °C and 400 °C, respectively. No liquid water remains stable at those temperatures. Thus, isotope partitioning between water and gas is not occurring, and N_2 remains unfractionated. Spring gases are vented at temperatures between 29 °C and 59 °C (Table 2), at temperatures where degassing is probably limited. In contrast, at Poás, the fumaroles are vented at ~100-150 °C (Fischer et al., 2015). At these temperatures, liquid and gaseous water are stable and water/gas partitioning can occur. These conditions are comparable to those observed for hydrothermal gases from Iceland or Yellowstone, where negative $\delta^{15}N$ values were previously observed in conjunction with air like Δ_{30} values (Labidi et al., 2020). Our conclusion is also consistent with the observation of sporadically negative $\delta^{15}N$ (with no available Δ_{30} data) in Poás fumaroles sampled in 2001. Values as low as ~−3.0‰ were observed in fumarole vented at temperature between 76 and 108 °C (Fischer et al., 2002). In other fumaroles (89-101 °C) sampled between 1998 and 2001, while unfractionated air-like $\delta^{15}N$ and N_2/Ar values were reported (Vaselli et al., 2003). More work is warranted to follow the potential Δ_{30}–$\delta^{15}N$ evolution of a given fumarole through time, but in the interim, we suggest caution in interpreting $\delta^{15}N$ data at Poás in the absence of Δ_{30}.

5.3. Is high-temperature nitrogen also fractionated?

Whether high-temperature components with $\Delta_{30} \sim 0$‰ also experience $\delta^{15}N$ isotope fractionation in hydrothermal systems is an open question. At Momotombo, fumaroles have a high-temperature endmember with $\delta^{15}N$ ~+5‰ (Fig. 2). There, vent temperatures are >700 °C. This precludes liquid water to exist even at depths, ruling out the possibility of any water/gas isotope exchange. This is consistent with a previous observation of unfractionated $\delta^{15}N$ for fumaroles when they are vented at >300 °C (Fischer et al., 2005). At Poás however, the interpretation is not as straightforward, where the high-temperature endmember has a $\delta^{15}N$ ~+1‰ (Fig. 2), which is lower than at Momotombo by ~4‰, implying that a fractionation similar to that for the air component could have occurred. It is conceivable that high-T volatiles have been delivered to the water table *prior to* hydrothermal degassing, where they would experience $^{15}N/^{14}N$ fractionation together with the air-derived gases. In this interpretation, the high-T $\delta^{15}N$ value of ~+1‰ obtained by extrapolation to $\Delta_{30} = 0$ would not record the actual magmatic $\delta^{15}N$ value at Poás, and the Poás trend would be parallel to the main array as the result of a fractionation equally affecting both the atmospheric and high-T volatiles. However, with our dataset alone, we cannot exclude that high-T volatiles had been delivered to the fumaroles *after* hydrothermal degassing. If so, the Poás high-T endmember could be truly unique in $\delta^{15}N$, and the Poás trend being parallel to the main array (Fig. 2) would be fortuitous. This latter scenario relies on a coincidence, and thus appears unlikely, although it cannot be fully ruled out.

5.4. N_2/Ar ratios place independent constraints on hydrothermal degassing

The solubilities of argon and nitrogen are distinct by about a factor of 2 in geothermal waters at temperatures between 20 and 100 °C (Ballentine et al., 2002). Thus, water/gas processes may be tracked with N_2/Ar ratios, independently of nitrogen isotopes. Low N_2/Ar ratios for air-like Δ_{30} values are observed at Poás, while most other samples have near-air values for N_2/Ar at air-like Δ_{30} (Fig. 4), confirming that at Poás liquid-gas partitioning occurred in the sub-surface. We can again use a Rayleigh fractionation calculation to infer the amount of degassing implied by the N_2/Ar ratio data, where

$$N_2/Ar = (N_2/Ar)_0 f^{\alpha-1} \quad (1)$$

and

$$\alpha = (K_{N_2}/K_{Ar}), \quad (2)$$

where f is the fraction of remaining Ar in the water, $(N_2/Ar)_0$ the known starting composition of ASW, and α is the fractionation coefficient given for a gas/liquid system given by Equation (2), and K_i is the Henry's-law constant for species i, as compiled in Ballentine et al. (2002). Taking $(N_2/Ar)_0$ to be 41, we find that the lowest N_2/Ar value of ~10 implied by our data occurs for about 94% degassing of N_2 (75% degassing of Ar) prior to sampling (Fig. 4). To first order, this degree of degassing is consistent with estimates made on the basis of $^{15}N/^{14}N$ values (section 5.2).

There is a caveat to this interpretation. Data for $\delta^{15}N$ and N_2/Ar appear consistent with fractionation within hydrothermal systems, but no direct correlation is observed between $\delta^{15}N$ and N_2/Ar (Table 1). This is perhaps because degassing may yield variable $^{15}N/^{14}N$ and N_2/Ar fractionations depending on the exact temperature and pressure conditions (Lee et al., 2015; Warr et al., 2015). Under conditions making the gas behavior non-ideal, degassing may change the N_2-Ar solubility relationship, as suggested for heavier noble gases (Labidi et al., 2020; Warr et al., 2015). Additionally, small contributions of high-temperature volatiles are likely to cause shifts in $\delta^{15}N$ with no obvious increases in N_2/Ar ratios (Fig. 4). This is because high-temperature endmembers with $\Delta_{30} = 0‰$ appear to have N_2/Ar and $N_2/^{36}Ar$ ratios of ~100 and ~10^4, respectively (Fig. 4). These values are essentially similar to air, consistent with pioneer work on the CAVA (Hilton et al., 2002; Snyder et al., 2003), but remain lower than volcanic endmembers at other arcs (Taran, 2009; Zelenski and Taran, 2011). We note that one of the Momotombo fumaroles has a high N_2/Ar of ~500, higher than other high-temperature gases by a factor of 5. The significance of variable N_2/Ar ratios in Central American high-temperature endmembers must be systematically investigated in future work, with Δ_{30} data.

5.5. $\delta^{15}N$-N_2/He relationships constrained by Δ_{30} data

In contrast to argon, the solubility of helium in geothermal waters is nearly indistinguishable from that of nitrogen in the relevant temperature range (Ballentine et al., 2002). Data can be accounted for by mixing between air and an endmember with $N_2/^3He$ ratios ~10^8 (Fig. 5). This is higher than MORB gases that are characterized by $N_2/^3He$ ratios of about 10^6 (Javoy and Pineau, 1991; Marty and Zimmermann, 1999). The Poás fumaroles involve a mixing scenario that is similar to the one for Momotombo, involving high-T endmembers with a $N_2/^3He$ of ~10^8 (Fig. 5). This observation argues against a significant contribution of MORB derived volatiles to Poás volcanic gas discharges. Overall light $\delta^{15}N$ values from Poás were previously suggested to reflect a contribution from MORB-derived volatiles, contrary to the majority of other CAVA gas discharges that showed predominantly slab-derived N (Fischer et al., 2002; Elkins et al., 2006). Our new Δ_{30} data suggest a revision to the interpretation of ^{15}N depletions and show that they rather reflect contributions of fractionated air (Fig. 2) mixed with a predominantly non-MORB magmatic component with elevated N_2/He ratios (Fig. 5).

5.6. Magmatic endmembers throughout the arc are enriched in N_2

In an attempt to characterize subduction volatiles, we constrain the high-temperature endmembers for nitrogen isotopes and N_2/Ar, N_2/He, He/Ne and He/Ar ratios. Endmember compositions are calculated assuming two-component mixing with air constrained by Δ_{30} values, as described above. We focus on fumarole data to constrain endmember compositions, since they show the lowest Δ_{30} and no evidence of crustal contamination (see supplementary discussion).

The derived N_2/He ratios are higher than MORB by two orders of magnitude. In contrast, He/Ne, He/Ar and $N_2/^{36}Ar$ are all lower than MORB by two to three orders of magnitude (Fig. 4–6). The simplest explanation is that slab-derived N_2, Ne and Ar were added to a depleted mantle source with an unmodified helium signature (Fig. 7). A straightforward quantification of slab-derived N_2, Ar and Ne to the mantle wedge is possible using $N_2/^3He$, $^3He/^{22}Ne$ and $^3He/^{36}Ar$ ratios. This approach is viable if ^3He subduction is negligible (Staudacher and Allegre, 1988), notwithstanding that slab components are required to contribute minute ^4He ingrowth from subducted uranium (Hilton et al., 2002).

The high-T, arc magma endmembers at Poás and Momotombo have $N_2/^3He$ ratios two orders of magnitude higher than MORB, requiring nitrogen addition to mantle sources in these arc systems. Sedimentary nitrogen may be a straightforward contributor to the Momotombo source, explaining the high $\delta^{15}N$ of + 5‰ there (Fig. 7). Sediments on the modern oceanic crust directly offshore of Central America are likely candidates, since they have an average $\delta^{15}N$ of ~5‰ (Li and Bebout, 2005). Poás volcano is more complicated, because the lower $\delta^{15}N$ (Fig. 2) may not be a genuine representation of the Poás mantle source. We note that because $N_2/^3He$ are indistinguishable between Poás and Momotombo, they must have received a comparable amount of slab-derived N.

Sub-arc magmatic endmembers have lower $^3He/^{22}Ne$ and $^3He/^{36}Ar$ ratios by 2 to 3 orders of magnitude compared to those of MORBs. Like nitrogen, this likely requires substantial addition of slab-derived neon and argon to a mantle source. Samples with near-zero Δ_{30} have $^{22}Ne/^{36}Ar$ lower than both MORB and air by one to two orders of magnitude (Table 1), with values trending toward ~0.7×10^{-2}. This is similar to the median ratio of an entire section of altered oceanic crust and sediments of ~1×10^{-2} (Chavrit et al., 2016). The similarity in $^{22}Ne/^{36}Ar$ between the magmatic endmembers at CAVA and the slab is consistent with a mantle wedge being overwhelmed by the addition of slab-derived neon and argon. Samples with near-zero Δ_{30} also have atmospheric $^{40}Ar/^{36}Ar$ values (Table 1), indicating that Ar from the mantle wedge has retained the noble gas isotopic signature of its subducted atmospheric source. This is likely explained by the contribution of surface-derived argon with atmospheric $^{40}Ar/^{36}Ar$ ratios to the mantle wedge. This sheds new light on atmospheric $^{40}Ar/^{36}Ar$ observed systematically in all known Central American fumaroles (Snyder et al., 2003) and essentially all gas discharges sampled to date from subduction zones (Hilton et al., 2002; Sano and Fischer, 2013): A likely origin for the atmospheric Ar in high-T endmembers is devolatilizing subducted protoliths that are otherwise known to have atmospheric Ar isotopic signatures (Chavrit et al., 2016; Holland and Ballentine, 2006; Staudacher and Allègre, 1988). Our high-T data shows that not all of the subducted air-derived Ar is transferred into the deeper mantle and that some of it is released via arc volcanism. Our data also dispels the notion that atmospheric Ar-isotope signatures of arc-gases are exclusively the result of shallow atmospheric contamination in the hydrothermal system.

5.7. Revisiting volatile fluxes in the central American subduction zone

The perspective that volatiles from the mantle wedge incorporate recycled argon is problematic, as it limits the use of nitrogen excesses, N_2^*, calculated on the basis of N_2/Ar ratios (Fischer et al., 2002; Hilton et al., 2002). We show here that magmatic volatiles deliver measurable amounts of argon (with atmospheric $^{40}Ar/^{36}Ar$) to the fumaroles. Consequently, assumptions on N_2^* may naturally underestimate the outgassing flux of N_2. Estimates for the fluxes of N_2, Ar, and Ne can be obtained from ^3He degassing fluxes. Using a combination of S/CO_2, He/CO_2 and $^3He/^4He$ ratios, and an SO_2 flux of 21.3×10^9 mol/yr, Hilton et al. (2002) derived a ^3He flux of 5.4 mol/yr for the entire CAVA. Using the CAVA CO_2 flux from Fischer et al. (2002) of 94×10^9 mol/yr, and a $CO_2/^3He$ ratio of 210^{10}

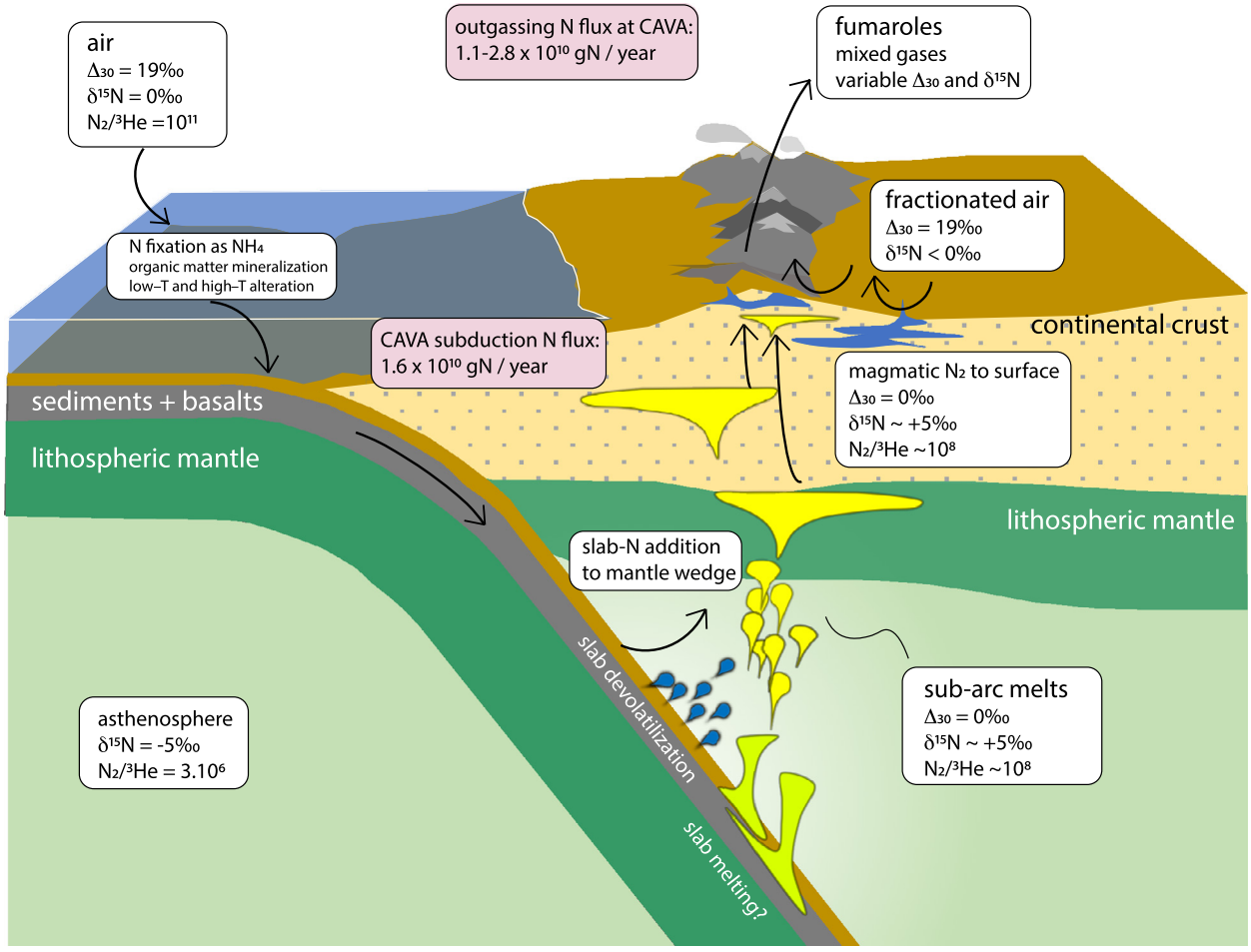

Fig. 7. Cartoon representing various processes and reservoirs constrained in this study. Scales are grossly exaggerated, especially for melt conduits and magma chambers. A slab with sediments, basalts, and oceanic lithospheric mantle is shown to enter subduction. The slab composition is not constrained here but is likely enriched in all volatiles relative to ^{3}He (Busigny et al., 2019; Chavrit et al., 2016). In the slab, nitrogen is fixed as NH_4^+ (Busigny et al., 2019 and references therein) so no Δ_{30} values are defined; Δ_{30} is only relevant for N_2 molecules. Both slab devolatilization and slab melting are shown for illustration. Any slab melting would be relevant underneath Costa Rica (Hoernle et al., 2008) while slab devolatilization and sediment-derived fluids would contribute to sources underneath Nicaragua and El Salvador (Patino et al., 2000). The melting region is characterized as the high-temperature endmembers constrained in this work (Fig. 7). Melts and super-critical fluids are suggested to host dissolved N_2 (Libourel et al., 2003; Mikhail and Sverjensky, 2014). Upon partial melting of a NH_3-bearing mantle source, magmatic N_2 would form with a Δ_{30} of 0‰. The high-T N_2 is then contributed to hydrothermal systems in the sub-surface by near-quantitative magmatic degassing. Air circulation in the sub-surface allows air-saturated waters to undergo degassing, and subsequent gas release with fractionated compositions.

(Kagoshima et al., 2015), we obtain a ^{3}He flux 4.7 mol/yr. Here, we take a ^{3}He flux of 5.0 mol/yr for the sake of illustration. We combine our new elemental ratios estimates for the CAVA source (Fig. 4–6) with ^{3}He fluxes to derive new estimates for N_2, ^{36}Ar, and ^{22}Ne outgassing fluxes in the central American arc.

We derive $N_2/^{3}He$ ratios between 8×10^{7} and 2×10^{8} for magmatic volatiles in Central America (Fig. 5), from samples with $\Delta_{30} < 5$‰. This results in a N_2 flux between 4.0×10^{8} and 1.0×10^{9} mol N_2/y (or 1.1×10^{10} and 2.8×10^{10} g N/y). This range for the nitrogen mass flux is higher than previous estimates of 8.2×10^{9} g N/y (Fischer et al., 2002; Hilton et al., 2002). Our derived range of nitrogen fluxes overlaps the estimated flux of subducting nitrogen of 1.6×10^{10} g N/y (1.1×10^{9} mol N/y, or 5.7×10^{8} mol N_2/yr), given with no uncertainty in Busigny et al. (2019) and Li and Bebout (2005). This suggests that in the Central American subduction zone, the N_2 cycle is not required to be out of equilibrium. Instead, the revisited fluxes being identical within uncertainty, they allow N_2 to be quantitatively recycled through the mantle wedge and returned to the surface by degassing rather than being delivered to the deep mantle. An additional source of outgassing underestimation, here, is that we ignore forearc devolatilization for N_2, known to occur in the CAVA (Inguaggiato et al., 2004). Future work will be necessary to constrain this fraction of the N_2 flux that will inevitably increase the outgassing flux further. In any case, our newly defined N_2 outgassing fluxes are high, and in the range of subducting fluxes. Because this subduction zone is relatively "warm" and therefore more similar to subduction zones in the past over geological timescales (Keller and Schoene, 2018; Martin and Moyen, 2002), the finding that nitrogen is recycled by subduction and arc magmatism in the Central American system suggests that nitrogen subduction could have been inefficient through geological time. This conclusion is also in agreement with recent experimental work suggesting warm subduction zones limit nitrogen recycling in the deep mantle (Jackson et al., 2021).

We estimate the $^{3}He/^{36}Ar$ of magmatic inputs to be $\sim 10^{-4}$ (Fig. 6). A $^{3}He/^{36}Ar$ ratio of $\sim 10^{-4}$ leads to a degassing ^{36}Ar flux of $\sim 5.0 \times 10^{4}$ mol/y (1.8×10^{6} g ^{36}Ar/y) in Central America. Using 1.4×10^{16} g of subducted crust, depths of ~6 km of oceanic crust and ~500 m of sediments, and the noble gases abundances in the oceanic crust (Chavrit et al., 2016), we derive a ^{36}Ar subduction flux of 1.1×10^{8} cm^{3} STP/y, or 4.5×10^{4} mol ^{36}Ar/y. Because of the large uncertainties in ^{36}Ar concentrations in rocks (Chavrit et al., 2016), this subduction flux estimate is probably associated with a ~50% uncertainty, and is presented here for illustration only. We note however that subduction and outgassing ^{36}Ar flux compare favorably. Like nitrogen, our flux analysis seems to allow quantita-

tive release of slab-derived ^{36}Ar to the mantle wedge, which would not require substantial ^{36}Ar recycling into the deep mantle in this subduction zone. The same conclusion holds for neon. Using a $^{3}He/^{22}Ne$ of $\sim 2 \times 10^{-2}$ (Fig. 6), we obtain a ^{22}Ne degassing flux of $\sim 2.5 \times 10^{2}$ mol/y (5.5×10^{3} g ^{22}Ne/y). The $^{22}Ne/^{36}Ar$ of subducting components is largely variable, around a mode of $\sim 10^{-2}$ (Chavrit et al., 2016). This yields a ^{22}Ne subduction flux of 1.1×10^{6} cm^{3} STP/y, or 4.5×10^{2} mol ^{22}Ne/y. Again, although large uncertainties must be taken into consideration, the neon subduction and degassing fluxes appear equivalent, arguing in favor of quantitative ^{22}Ne recycling in the central American subduction zone back to the surface.

The simplest interpretation of the fluxes derived here is that the Central American subduction zone acts as a subduction barrier for N, Ar, and Ne: volcanic fluxes for N_2, Ar, and Ne, determined with the $^{15}N^{15}N$ approach, *no longer require* subduction of these elements past the sub-arc melting region in the central American subduction zone.

6. Conclusion

Gas discharges in Central America are volatile mixtures involving contributions from at least three endmembers: air (±fractionated air), crust, and mantle-derived components. Using Δ_{30} as a tracer of nitrogen from air in fumaroles and springs, we show that O_2/N_2 ratios are unreliable tracers of air in these systems. We also show that $\delta^{15}N$ and N_2/Ar ratios experienced fractionation during water degassing at depth, rendering these unreliable as signatures of air where liquid water is thermodynamically stable. This is problematic since the degassing fractionation may lead to $\delta^{15}N$ values that insidiously mimic MORB gases. This does not seem to affect magmatic components, but more work is needed on Poás – where interaction with the hydrothermal system may be significant, before a firm conclusion can be reached. A preliminary conclusion is that without Δ_{30} data, the $\delta^{15}N$-N_2-Ar systematics may be deceptive, and can lead to confusion with regard to the origin of N_2 in mixed gases.

We derive estimates of N_2/He, He/Ar and He/Ne ratios that reliably exclude atmospheric components. N_2, Ar and Ne enrichments by two or three orders of magnitude compared to a MORB source are observed. They are attributed to mantle wedge sources incorporating slab-derived gases. Using known ^{3}He degassing fluxes, we calculated N_2, Ne and Ar degassing fluxes for the Central American arc that could balance subduction fluxes, within uncertainties, no longer requiring the Central American arc to have heavily imbalanced volatile cycles.

CRediT authorship contribution statement

Jabrane Labidi: $^{15}N^{15}N$ data acquisition, interpretation, figures and manuscript writing. **Edward Young:** Contribution to the $^{15}N^{15}N$ data acquisition, figures and manuscript editing. **Tobias Fischer:** Field work, $^{40}Ar/^{36}Ar$ data acquisition on fumaroles, manuscript editing. **Peter Barry:** Field work, noble gases data on springs, manuscript editing. **Chris Ballentine:** Support for noble gases data on springs, manuscript editing. **Marteen De Moor:** Field work, bulk chemistry data on springs.

Declaration of competing interest

The authors declare that they have no known competing financial interests or personal relationships that could have appeared to influence the work reported in this paper.

Acknowledgement

This study was supported by the Deep Carbon Observatory through Sloan Foundation grant numbers G-2018-11346 to EDY. This work was also supported by grant G-2016-7206 from the Alfred P. Sloan Foundation to PHB. Karen Lloyd and Donato Giovannelli are thanked for co-organizing the Subduction meets Biology initiative. Further, we acknowledge the National Science Foundation (NSF) award MGG-2015789 to PHB. We thank Yuri Taran and an anonymous reviewer for constructive and helpful comments. Rosemary Hickey-Vargas is thanked for editorial handling.

Appendix A. Supplementary material

Supplementary material related to this article can be found online at https://doi.org/10.1016/j.epsl.2021.117112.

References

Ballentine, C.J., Burgess, R., Marty, B., 2002. Tracing fluid origin, transport and interaction in the crust. Rev. Mineral. Geochem. 47 (1), 539–614.
Barry, P.H., Lawson, M., Meurer, W.P., Warr, O., Mabry, J.C., Byrne, D.J., Ballentine, C.J., 2016. Noble gases solubility models of hydrocarbon charge mechanism in the Sleipner Vest gas field. Geochim. Cosmochim. Acta 194, 291–309.
Bebout, G.E., Fogel, M.L., 1992. Nitrogen-isotope compositions of metasedimentary rocks in the Catalina Schist, California: implications for metamorphic devolatilization history. Geochim. Cosmochim. Acta 56 (7), 2839–2849.
Bebout, G.E., Agard, P., Kobayashi, K., Moriguti, T., Nakamura, E., 2013. Devolatilization history and trace element mobility in deeply subducted sedimentary rocks: evidence from Western Alps HP/UHP suites. Chem. Geol. 342, 1–20.
Bekaert, D.V., Turner, S.J., Broadley, M.W., Barnes, J.D., Halldórsson, S.A., Labidi, J., Wade, J., Walowski, K.J., Barry, P.H., 2021. Subduction-driven volatile recycling: a global mass balance. Annu. Rev. Earth Planet. Sci. 49.
Busigny, V., Cartigny, P., Laverne, C., Teagle, D., Bonifacie, M., Agrinier, P., 2019. A reassessment of the nitrogen geochemical behavior in upper oceanic crust from Hole 504B: implications for subduction budget in Central America. Earth Planet. Sci. Lett. 525, 115735.
Busigny, V., Cartigny, P., Philippot, P., Ader, M., Javoy, M., 2003. Massive recycling of nitrogen and other fluid-mobile elements (K, Rb, Cs, H) in a cold slab environment: evidence from HP to UHP oceanic metasediments of the Schistes Lustrés nappe (western Alps, Europe). Earth Planet. Sci. Lett. 215, 27–42. https://doi.org/10.1016/s0012-821x(03)00453-9.
Carr, M.J., Feigenson, M.D., Patino, L.C., Walker, J.A., 2003. Volcanism and geochemistry in Central America: progress and problems. Geophys. Monogr. Geophys. Union 138, 153–174.
Chavrit, D., Burgess, R., Sumino, H., Teagle, D.A.H., Droop, G., Shimizu, A., Ballentine, C.J., 2016. The contribution of hydrothermally altered ocean crust to the mantle halogen and noble gas cycles. Geochim. Cosmochim. Acta 183, 106–124.
De Leeuw, G.A.M., Hilton, D.R., Fischer, T.P., Walker, J.A., 2007. The He–CO2 isotope and relative abundance characteristics of geothermal fluids in El Salvador and Honduras: new constraints on volatile mass balance of the Central American volcanic arc. Earth Planet. Sci. Lett. 258, 132–146.
Elkins, L.J., Fischer, T.P., Hilton, D.R., Sharp, Z.D., McKnight, S., Walker, J., 2006. Tracing nitrogen in volcanic and geothermal volatiles from the Nicaraguan volcanic front. Geochim. Cosmochim. Acta 70, 5215–5235.
Fischer, T.P., Hilton, D.R., Zimmer, M.M., Shaw, A.M., Sharp, Z.D., Walker, J.A., 2002. Subduction and recycling of nitrogen along the Central American margin. Science 297, 1154–1157.
Fischer, T.P., Ramírez, C., Mora-Amador, R.A., Hilton, D.R., Barnes, J.D., Sharp, Z.D., Le Brun, M., de Moor, J.M., Barry, P.H., Füri, E., Shaw, A.M., 2015. Temporal variations in fumarole gas chemistry at Poás volcano, Costa Rica. J. Volcanol. Geotherm. Res. 294, 56–70. https://doi.org/10.1016/j.jvolgeores.2015.02.002.
Fischer, T.P., Takahata, N., Sano, Y., Sumino, H., Hilton, D.R., 2005. Nitrogen isotopes of the mantle: insights from mineral separates. Geophys. Res. Lett. 32.
Gazel, E., Carr, M.J., Hoernle, K., Feigenson, M.D., Szymanski, D., Hauff, F., Van Den Bogaard, P., 2009. Galapagos-OIB signature in southern Central America: mantle refertilization by arc–hot spot interaction. Geochem. Geophys. Geosyst. 10.
Giggenbach, W.F., 1992. Isotopic shifts in waters from geothermal and volcanic systems along convergent plate boundaries and their origin. Earth Planet. Sci. Lett. 113 (4), 495–510.
Hilton, D.R., Fischer, T.P., Marty, B., 2002. Noble gases and volatile recycling at subduction zones. Rev. Mineral. Geochem. 47, 319–370.
Hilton, D.R., Ramirez, C.J., Mora-Amador, R., Fischer, T.P., Füri, E., Barry, P.H., Shaw, A.M., 2010. Monitoring of temporal and spatial variations in fumarole helium and carbon dioxide characteristics at Poás and Turrialba volcanoes, Costa Rica (2001-2009). Geochem. J. 44, 431–440.

Hoernle, K., Abt, D.L., Fischer, K.M., Nichols, H., Hauff, F., Abers, G.A., Van Den Bogaard, P., Heydolph, K., Alvarado, G., Protti, M., 2008. Arc-parallel flow in the mantle wedge beneath Costa Rica and Nicaragua. Nature 451, 1094–1097.

Holland, G., Ballentine, C.J., 2006. Seawater subduction controls the heavy noble gas composition of the mantle. Nature 441, 186–191. https://doi.org/10.1038/nature04761.

Inguaggiato, S., Taran, Y., Grassa, F., Capasso, G., Favara, R., Varley, N., Faber, E., 2004. Nitrogen isotopes in thermal fluids of a forearc region (Jalisco Block, Mexico): evidence for heavy nitrogen from continental crust. Geochem. Geophys. Geosyst. 5.

Jackson, C.R.M., Cottrell, E., Andrews, B., 2021. Warm and oxidizing slabs limit ingassing efficiency of nitrogen to the mantle. Earth Planet. Sci. Lett. 553, 116615.

Javoy, M., Pineau, F., 1991. The volatiles record of a "popping" rock from the Mid-Atlantic Ridge at 14°N: chemical and isotopic composition of gas trapped in the vesicles. Earth Planet. Sci. Lett. 107, 598–611.

Kagoshima, T., Sano, Y., Takahata, N., Maruoka, T., Fischer, T.P., Hattori, K., 2015. Sulphur geodynamic cycle. Sci. Rep. 5 (1), 1–6.

Keller, B., Schoene, B., 2018. Plate tectonics and continental basaltic geochemistry throughout Earth history. Earth Planet. Sci. Lett. 481, 290–304.

Kennedy, B.M., Hiyagon, H., Reynolds, J.H., 1991. Noble gases from Honduras geothermal sites. J. Volcanol. Geotherm. Res. 45, 29–39.

Labidi, J., Barry, P.H., Bekaert, D.V., Broadley, M.W., Marty, B., Giunta, T., Warr, O., Lollar, B.S., Fischer, T.P., Avice, G., 2020. Hydrothermal 15 N 15 N abundances constrain the origins of mantle nitrogen. Nature 580, 367–371.

Lee, H., Fischer, T.P., Muirhead, J.D., Ebinger, C.J., Kattenhorn, S.A., Sharp, Z.D., Kianji, G., Takahata, N., Sano, Y., 2017. Incipient rifting accompanied by the release of subcontinental lithospheric mantle volatiles in the Magadi and Natron basin, East Africa. J. Volcanol. Geotherm. Res. 346, 118–133.

Lee, H., Sharp, Z.D., Fischer, T.P., 2015. Kinetic nitrogen isotope fractionation between air and dissolved N2 in water: implications for hydrothermal systems. Geochem. J. 49, 571–573.

Lee, J.-Y., Marti, K., Severinghaus, J.P., Kawamura, K., Yoo, H.-S., Lee, J.B., Kim, J.S., 2006. A redetermination of the isotopic abundances of atmospheric Ar. Geochim. Cosmochim. Acta 70, 4507–4512.

Li, L., Bebout, G.E., 2005. Carbon and nitrogen geochemistry of sediments in the Central American convergent margin: insights regarding subduction input fluxes, diagenesis, and paleoproductivity. J. Geophys. Res., Solid Earth 110.

Libourel, G., Marty, B., Humbert, F., 2003. Nitrogen solubility in basaltic melt. Part I. Effect of oxygen fugacity. Geochim. Cosmochim. Acta 67, 4123–4135. https://doi.org/10.1016/s0016-7037(03)00259-x.

Martin, H., Moyen, J.-F., 2002. Secular changes in tonalite-trondhjemite-granodiorite composition as markers of the progressive cooling of Earth. Geology 30, 319–322.

Marty, B., Dauphas, N., 2003. The nitrogen record of crust–mantle interaction and mantle convection from Archean to present. Earth Planet. Sci. Lett. 206 (3–4), 397–410.

Marty, B., Humbert, F., 1997. Nitrogen and argon isotopes in oceanic basalts. Earth Planet. Sci. Lett. 152, 101–112.

Marty, B., Zimmermann, L., 1999. Volatiles (He, C, N, Ar) in mid-ocean ridge basalts: Assesment of shallow-level fractionation and characterization of source composition. Geochim. Cosmochim. Acta 63 (21), 3619–3633.

Mikhail, S., Sverjensky, D.A., 2014. Nitrogen speciation in upper mantle fluids and the origin of Earth's nitrogen-rich atmosphere. Nat. Geosci. 7, 816–819. https://doi.org/10.1038/ngeo2271. http://www.nature.com/ngeo/journal/v7/n11/abs/ngeo2271.html#supplementary-information.

Moreira, M., Kunz, J., Allegre, C., 1998. Rare gas systematics in popping rock: isotopic and elemental compositions in the upper mantle. Science 279, 1178–1181.

Mukhopadhyay, S., 2012. Early differentiation and volatile accretion recorded in deep-mantle neon and xenon. Nature 486, 101–104. https://doi.org/10.1038/nature11141.

Patino, L.C., Carr, M.J., Feigenson, M.D., 2000. Local and regional variations in Central American arc lavas controlled by variations in subducted sediment input. Contrib. Mineral. Petrol. 138, 265–283.

Peacock, S.M., van Keken, P.E., Holloway, S.D., Hacker, B.R., Abers, G.A., Fergason, R.L., 2005. Thermal structure of the Costa Rica–Nicaragua subduction zone. Phys. Earth Planet. Inter. 149, 187–200.

Plank, T., Kelley, K.A., Zimmer, M.M., Hauri, E.H., Wallace, P.J., 2013. Why do mafic arc magmas contain ∼4 wt% water on average? Earth Planet. Sci. Lett. 364, 168–179.

Ranero, C.R., von Huene, R., 2000. Subduction erosion along the Middle America convergent margin. Nature 404, 748–752.

Raquin, A., Moreira, M.A., Guillon, F., 2008. He, Ne and Ar systematics in single vesicles: mantle isotopic ratios and origin of the air component in basaltic glasses. Earth Planet. Sci. Lett. 274, 142–150.

Sano, Y., Fischer, T.P., 2013. The analysis and interpretation of noble gases in modern hydrothermal systems. In: The Noble Gases as Geochemical Tracers. Springer, Berlin, Heidelberg, pp. 249–317.

Sano, Y., Takahata, N., Nishio, Y., Fischer, T.P., Williams, S.N., 2001. Volcanic flux of nitrogen from the Earth. Chem. Geol. 171 (3–4), 263–271.

Schwarzenbach, E.M., Gill, B.C., Gazel, E., Madrigal, P., 2016. Sulfur and carbon geochemistry of the Santa Elena peridotites: comparing oceanic and continental processes during peridotite alteration. Lithos 252–253, 92–108. https://doi.org/10.1016/j.lithos.2016.02.017.

Snyder, G., Poreda, R., Fehn, U., Hunt, A., 2003. Sources of nitrogen and methane in Central American geothermal settings: Noble gas and 129I evidence for crustal and magmatic volatile components. Geochem. Geophys. Geosyst. 4, 1–28.

Staudacher, T., Allègre, C.J., 1988. Recycling of oceanic crust and sediments: the noble gas subduction barrier. Earth Planet. Sci. Lett. 89, 173–183.

Taran, Y.A., 2009. Geochemistry of volcanic and hydrothermal fluids and volatile budget of the Kamchatka–Kuril subduction zone. Geochim. Cosmochim. Acta 73, 1067–1094.

Vaselli, O., Tassi, F., Minissale, A., Montegrossi, G., Duarte, E., Fernandez, E., Bergamaschi, F., 2003. Fumarole migration and fluid geochemistry at Poás volcano (Costa Rica) from 1998 to 2001. Geol. Soc. (Lond.) Spec. Publ. 213, 247–262.

Warr, O., Rochelle, C.A., Masters, A., Ballentine, C.J., 2015. Determining noble gas partitioning within a CO2–H2O system at elevated temperatures and pressures. Geochim. Cosmochim. Acta 159, 112–125.

Yeung, L.Y., Li, S., Kohl, I.E., Haslun, J.A., Ostrom, N.E., Hu, H., Fischer, T.P., Schauble, E.A., Young, E.D., 2017. Extreme enrichment in atmospheric 15N15N. Sci. Adv. 3, eaao6741.

Young, E.D., Rumble III, D., Freedman, P., Mills, M., 2016. A large-radius high-mass-resolution multiple-collector isotope ratio mass spectrometer for analysis of rare isotopologues of O2, N2, CH4 and other gases. Int. J. Mass Spectrom. 401, 1–10.

Zelenski, M., Taran, Y., 2011. Geochemistry of volcanic and hydrothermal gases of Mutnovsky volcano, Kamchatka: evidence for mantle, slab and atmosphere contributions to fluids of a typical arc volcano. Bull. Volcanol. 73, 373–394.

Zimmer, M.M., Fischer, T.P., Hilton, D.R., Alvarado, G.E., Sharp, Z.D., Walker, J.A., 2004. Nitrogen systematics and gas fluxes of subduction zones: insights from Costa Rica arc volatiles. Geochem. Geophys. Geosyst. 5.